Suppression of the low-spin multiplet components in the 3p photoelectron spectra of atomic and solid 3d metals

A. von dem Borne, R. L. Johnson, B. Sonntag, M. Talkenberg, A. Verweyen, Ph. Wernet, and J. Schulz
II Institut für Experimentalphysik, Universität Hamburg, Luruper Chaussee 149, 22761 Hamburg, Germany

K. Tiedtke, Ch. Gerth, B. Obst, and P. Zimmermann
Institut für Atomare und Analytische Physik, Technische Universität Berlin, Hardenbergstrasse 36, 10623 Berlin, Germany

J. E. Hansen
Department of Physics and Astronomy, University of Amsterdam, Valckenierstraat 65, NL-1018 XE Amsterdam, The Netherlands
(Received 31 May 2000; published 11 October 2000)

The 3p photoelectron spectra of Cr, Mn, Fe, and Co atoms have been studied experimentally and theoretically. The 3p-3d interaction in the final ionic state gives rise to an LS multiplet structure spanning a binding-energy range of around 20 eV. The prominent high-spin components at low binding energies contrast with the broad and weak low-spin components at high binding energies. Term-dependent lifetime broadening by super-Coster-Kronig decays is the main cause of the almost complete suppression of the latter lines. The corresponding 3p photoelectron spectra of the metals display only a single broad asymmetric line. The influence of correlation on the 3p photoelectron spectra is shown to be less dramatic than in the case of the better known 3s photoelectron spectra. We show that, while the peculiarities in the 3s spectrum are caused by configuration interaction, the single-configuration approximation already provides the clue to the interpretation of the 3p spectrum.

PACS number(s): 32.80.Hd, 32.80.−t, 31.25.Jf

I. INTRODUCTION

In recent years the 3p photoelectron spectra of Cr, Mn, Fe, and Co have been widely used to obtain information about the electronic and magnetic structures of metals, compounds, surfaces, thin films, and multilayer systems (see [1–12] and references therein). In particular, spin-resolved photoemission and linear and circular dichroism in angle-resolved photoemission have proved to be powerful atom-specific probes. Interpretation of the experimental spectra has in most cases relied on atomic models, usually some variant of the independent electron model [1–15], while different schemes, e.g., cluster or ligand field models, have been used to take solid state effects into account. Due to the experimental difficulties there are only a few 3p photoelectron spectra of free atoms and ions known [16] compared to the situation for solids. The pioneering experiments on atoms have been limited to the 3p photoelectron spectra of Cr and Mn [17–20], which sublimate at relatively low temperatures [21]. The strong coupling of the 3p hole with the 3d electrons spreads the $3p^5 3d^n 4s^m$ multiplet over an energy range of approximately 20 eV (see, e.g., [10,15,17,19]). The experimental spectra published so far either suffer from insufficient energy resolution or do not cover the full multiplet [17–20,22], except for the recently published results on Ni [23]. In order to determine the multiplet splitting as well as the strength and the width of the different components, we studied the 3p photoelectron spectra of Cr, Mn, Fe, and Co atoms experimentally and theoretically. On the basis of this study we hope to provide a more reliable basis for assessing atomic effects in the solid state spectra. With this in mind, the 3p photoelectron spectra of Cr and Mn metals were also measured. In the past the 3p spectra of 3d transition metals have been studied less exhaustively than the 3s spectra. Both spectra are perturbed but, as we will show, the two spectra deviate in rather different ways from the independent particle picture. This is probably one reason that the 3p spectra are still less well understood.

In the analysis presented here we assume that photoionization and the subsequent Auger decay are two independent processes. This assumption is expected to hold for the high-spin states which decay fairly slowly but to be less reliable for the very fast decay of some of the low-spin states.

II. EXPERIMENT

The atomic photoelectron spectra were recorded with a Scienta SES 200 electron energy analyzer at the HASYLAB SX 700 and the BESSY I TGM 5 undulator beam lines. Photon energies varied between 110 and 278 eV. The monochromatized undulator radiation was focused on a beam of free atoms generated in an effusive furnace heated either resistively or by electron impact. The temperatures necessary for the creation of an atomic beam of sufficient particle density are about 1650 K for Cr, 1200 K for Mn and 1800 K for Fe and Co [21]. At these temperatures the ground states Cr $3d^5 4s\,^7S$, Mn $3d^5 4s^2\,^6S$, Fe $3d^6 4s^2\,^5D$, and Co $3d^7 4s^2\,^4F$ are populated almost exclusively. The electron energy analyzer accepted only electrons with an emission angle close to the magic angle of 54.7° with respect to the polarization axis of the undulator light. The photoelectron spectra were recorded at a fixed photon energy $h\nu$, while scanning the accelerating (retarding) lens voltage of the analyzer. The constant analyzer pass energy of 75 eV resulted in a bandwidth constant over the whole spectrum. All spectra were corrected

for the analyzer transmission. The total instrumental energy bandwidth [full width at half maximum (FWHM)] amounted to 270 meV for Cr, 300 meV for Mn, 700 meV for Fe, and 320 meV for Co. The monochromators were calibrated using well known photoelectron and Auger lines of rare gases. Auger lines and the $3d$ photoelectron lines were used to establish the binding-energy scale.

The photoelectron spectra of the Cr and Mn metals were determined at the HASYLAB FLIPPER II station. A clean Cr(100) surface was prepared under UHV conditions by sputtering and annealing of a Cr crystal. A thick layer of Mn was evaporated on a copper crystal. The electron spectra were recorded with a cylindrical mirror analyzer. The instrumental bandwidth (FWHM) achieved was 500 ± 100 meV.

III. THEORY

A spin dependence of the Auger decay rates is the clue to the appearance of the $3p$ spectrum, where the lowest LS multiplets have high values of the total spin S while the higher multiplets have smaller spin values and the difference in spin determines the decay rates. In the following we will use Mn to illustrate the situation. Since the $3s$ and $3p$ spectra behave rather differently we will start by reviewing the $3s$ spectra, which have been studied much more extensively than the $3p$ spectra.

The ground state in the Mn atom has, as mentioned, the electron configuration $3s^2 3p^6 3d^5 4s^2$. The $4s$ electrons will not influence the coupling and can be omitted from the term labels together with the filled inner shells. The half filled $3d$ shell, $3d^5$, has a ^6S state much lower than all other states in the $3d^5$ configuration (Hund's rule) and removing a 3s electron can lead only to $3s3p^6(3d^5\,{}^6S)\,{}^7S$ or ^5S terms as long as the coupling in the 3d shell is unchanged. Thus two photoelectron peaks are expected, separated by a distance determined by the exchange interaction between the $3s$ and $3d$ electrons. The orbitals corresponding to these two electrons are located in the same region of space and the exchange interaction between them is consequently considerable. This means that the distance between the two peaks is expected to be large. The relative intensity of the peaks is in this approximation determined by the statistical degeneracy of the two terms, i.e., $7/5 = 1.4$.

The energy separation and the relative strengths of the corresponding lines in the photoelectron spectra of atoms and solids [17,19,24], and references therein] strongly deviate from these predictions. In addition, further peaks were observed in the spectra which originally were ascribed to solid state screening but later were realized to be due to intra-atomic interactions [17]. The theoretical spectra could be reconciled with the experimental results only by taking into account strong intra-atomic configuration intraction (CI) [24–26]. The $3s$ spectrum has therefore a rather prominent place in the history of the use of atomic concepts in the interpretation of solid state spectra.

In the $3s$ spectrum, CI moves the $3s3p^6(3d^5\,{}^6S)\,{}^5S$ term closer to $3s3p^6(3d^5\,{}^6S)\,{}^7S$, which is much less perturbed. Configuration interaction distributes the $3s3p^6(3d^5\,{}^6S)\,{}^5S$ intensity over several ^5S states thus increasing the intensity ratio $3s3p^6(3d^5\,{}^6S)\,{}^7S/3s3p^6(3d^5\,{}^6S)\,{}^5S$ from 1.4 to more than 2 [25] in reasonable agreement with the observations [19].

The situation for the $3p$ spectrum is more complicated. Although removing a $3p$ electron in principle can lead only to $3p^5(3d^5\,{}^6S)\,{}^7P$ or ^5P terms, this time, in addition to the $(^6S)\,{}^5P$ term, there are two additional ^5P terms in the $3p^5 3d^5$ configuration, based on the $3d^5\,{}^4P$ and ^4D parents. These terms are connected to $(^6S)\,{}^5P$ via nondiagonal electrostatic matrix elements and all three terms can thus in principle be reached by photoionization of a $3p$ electron. Experimentally, a total of five peaks, including the ^7P, have been observed [19,24]. Only the last is strong and the lack of a second strong component has frustrated the identification of the other features so far. Due to the importance of CI for the $3s$ spectrum, it is reasonable to attempt a similar explanation for $3p$. However, CI turns out to be less important for the $3p$ spectrum. Instead we will show that the single-configuration approximation can explain the main features of the $3p$ spectrum although CI is important for a more detailed understanding.

We will distinguish two types of CI here which, for convenience, we will call ''strong'' and ''weak'' CI. Strong CI is associated with large interaction integrals, as found when there is good overlap between the interacting electrons, while weak CI covers the rest. Very good overlap is obtained if the electrons are associated with the same shell, i.e., have the same n value, and strong CI will here be restricted to this case. The $3s$ spectrum has long been recognized as a prominent case of strong CI. This is because the main part of the interaction is due to a $3s3p^6 3d^5 \rightarrow 3s^2 3p^4 3d^6$ excitation fulfilling the condition that all participating electrons have the same n value. However, what makes this excitation especially prominent is that the energy connected with the excitation is very small. In addition to this excitation there is of course a large number of excitations belonging to the category weak CI.

For the $3p$ spectrum, there is also at least one excitation, $3p^5 3d^5 \rightarrow 3p^3 3d^7$, for which the interaction integral is very large. Nevertheless, although this excitation belongs in the category strong CI as defined above, its effect on the spectrum is much smaller, since the excitation energy is considerably larger than for the $3s3p^6 3d^5 \rightarrow 3s^2 3p^4 3d^6$ excitation.

However, there is another difference between the $3s$ and $3p$ spectra, this one connected with the decay rate. This difference is already present in the single-configuration approximation. For the $3p$ spectrum, as we will see, super-Coster-Kronig (SCK) decay is allowed, in which two $3d$ electrons in the initial state are involved. One of the two electrons fills the $3p$ hole and the other is ejected to the continuum. However, while this mechanism is allowed for the quintet terms, it is not possible for the septet because the highest-spin state possible in the final $3p^6 3d^3 4s^2$ configuration is quartet when the three $3d$ electrons have their spins aligned. Coupling with the continuum electron makes quintet (and triplet) states possible but not septets. Therefore, as long as the initial state is a good septet, it cannot decay to $3p^6 3d^3 4s^2$ via the Coulomb interaction in a single-configuration approximation. The $3d^5\,{}^6S$ term is located well

below the quartet terms in $3d^5$ [27] so that this term, in fact, is very pure in the sextet label, and the same applies to the septet in $3p^5 3d^5$.

For the $3s$ spectrum, the same spin-selection rules apply but it turns out that in the $3s3p^6 3d^5 \rightarrow 3s^2 3p^6 3d^3\ \epsilon l$ decay even the ^5S term cannot decay by SCK since it is impossible to form a ^5S term by adding an *s*, *d*, or *g* electron to $3d^3$ terms because the $3d^3$ configuration has only *F* and *P* terms with quartet character. There is a second SCK decay possible for the $3s$ hole, namely, $3s3p^6 3d^5 \rightarrow 3s^2 3p^5 3d^4$ and this time both ^7S and ^5S terms can decay since both symmetries exist in the final state. Thus the linewidths of the two $3s$ peaks are of comparable size (although ^5S is somewhat wider; see below) which makes it much easier to compare intensities than for the $3p$ spectrum where the main ^5P peak turns out to be much wider than the ^7P peak as we will see. It is the last observation that provides the main justification for this paper. As mentioned, this effect is present in the single-configuration approximation, and a key result of this study is that the effect is so strong that it is not washed out by CI.

That the decay rates for the septet and quintet terms in the $3p$ spectrum are very different in a single-configuration approximation was realized by McGuire [28] quite some time ago. McGuire noted that a similar although much less pronounced effect was predicted in his calculations for the $3s$ spectrum. Although this effect is not caused by spin-selection rules, it is real, and we will in the following refer to it as an ''effective'' spin dependence. However, McGuire's paper is mainly concerned with showing that configuration interaction cancels the intrinsic difference between septet and quintet for the $3s$ spectra and he surmised that the same would happen for the $3p$ spectrum. This turns out to be incorrect, but only recently Kotani and collaborators [10,29,30] have rediscovered spin dependence, which can broaden the low spin states in the photoelectron spectra of both transition metal and rare earth elements. However, Malutzki *et al.* [18] had already discussed the possibility of the effect in 1985 and Schmidt [31] showed its existence in Mn in the same year, independently of McGuire's earlier results, but this publication also appears to have left no trace in the literature. Kotani and co-workers have discussed the effect in the rare earth elements [29] and the spectra of $NiCl_2$ [30] as well as in MnO and MnF_2 [10]. For the $3s$ spectrum many studies including CI have been reported [15,24–26,28] but McGuire's [28] suggestion that CI is equally important for the $3p$ spectrum has not been explored. Here we present such studies, showing that the effect of CI is much less dramatic for the $3p$ spectrum than for $3s$. In addition, we point out that the photon energy dependence of the photoionization cross sections further complicates the interpretation of the $3p$ spectrum.

A. Calculations

Although qualitative arguments, such as those sketched above, are useful for understanding the main features of the spectra, calculations are required in order to obtain quantitative agreement. Calculations of energies, photoionization probabilities, and Auger decay rates have been carried out using the suite of programs due to Cowan [32] in the approximately relativistic Hartree-Fock (HFR) approximately introduced by Cowan and Griffin [33], both with and without configuration interaction, CI, included. Although the main features can be explained within the single-configuration approximation (SCA), CI is nevertheless important for a detailed agreement between theory and experiment; in fact, the introduction of CI is indispensable for the agreement for the $3s$ spectrum and less important although by no means negligible for the $3p$ spectrum. CI calculations of the Auger decay rates have been carried out for Mn only. The decay rates in Cr are expected to follow the same trend and the open $4s$ shell makes such calculations less tractable for Cr. However, CI calculations have been carried out for the energy and excitation spectrum of Cr since the single-configuration approach does not explain all observed peaks in this spectrum.

B. Energies

It is well known that single-configuration calculations do not give the correct spread of a configuration. This is true even when strong CI is included. In general the calculated spread is larger than observed, and this has been understood as the result of the cumulative effect of weak CI with the large number of high-lying configurations [34], which will press the upper terms down more than the lower ones, thereby contributing to a compression of the width of the configuration. In this case the effect is easy to visualize since low-spin states will be much more numerous in the spectrum than high-spin states. The same actually applies to the strong CI effects in this case, as noticed earlier [26]. The compression can be described phenomenologically by reducing the size of the HF, alternately HFR, Slater integrals (adding in principle ''Slater'' integrals of odd rank also [34]) and this ''scaling'' is widely used to approximate weak CI, which is very difficult to calculate *ab initio* for a many-electron atom with several open shells such as Mn. The scaling factors are, of course, different in principle according to whether strong CI effects are included explicitly or not. The explicit inclusion of strong CI together with the implicit inclusion of weak CI via scaling factors is expected to be the most accurate semiempirical approach. For both Mn and Cr we have used this method with scaling factors equal to 80% for the direct and exchange Slater integrals, while the spin-orbit interaction and the electrostatic CI integrals were used without scaling. These scaling factors correspond well to what is found for other configurations in these atoms [32], and the same set of scaling factors has in fact been used both in the single-configuration and in the CI calculations. Results for Mn are shown in Table II and for Cr in Table III below. It is, of course, an approximation to assume that one scaling factor can bring all terms into agreement with experiment, and the remaining disagreements between observed and calculated energies are small enough that they might be due to this approximation.

C. Decay rates

We present both single-configuration and CI calculations for Mn where the SCA is used to label results obtained using

TABLE I. Calculated Coster-Kronig and super-Coster-Kronig decay rates (in s^{-1}, numbers in square brackets are powers of 10) and total line widths (FWHM in eV) of Mn II $3p$ hole states. A single configuration, and a configuration interaction approximation are shown. Decay via p and f electrons is included. The states are given in order of increasing energy. The values shown are averages over individual J levels; see text. ''Direct'' indicates the $3p^5 3d^5 4s^2 \rightarrow 3p^5 3d^5 4s$ decay, which is possible only for the high-lying (^6S) ^5P term as discussed in the text.

	SCA				CI		
Mn II state	CK	SCK	Direct	Width	CK	SCK	Width
$3p^5(3d^5\,{}^6S)4s^2\,{}^7P$	4.8[13]	5.7[10]		0.031	1.9[14]	1.7[11]	0.13
$3p^5(3d^5\,{}^4D)4s^2\,{}^5P$	6.6[13]	9.0[13]		0.10	3.3[14]	5.1[13]	0.25
$3p^5(3d^5\,{}^4P)4s^2\,{}^5P$	5.8[13]	2.4[14]		0.19	8.9[14]	1.9[14]	0.71
$3p^5(3d^5\,{}^6S)4s^2\,{}^5P$	7.6[14]	2.9[15]	3.2[14]	2.6	7.4[14]	2.8[15]	2.5 [a]

[a]Includes ''direct'' SCA contribution (column 4).

single-configuration HFR calculations for the initial and final states. Since HFR is a relativistic approach, these calculations employ intermediate coupling although the actual coupling for the high-spin states is close to LS. Table I shows the result of calculations of CK and SCK decay rates for Mn. The calculations include decays for p, f, and h continuum electrons where the h decay (present for SCK only) is negligible (around 1×10^{10} s^{-1}). The coupling between the continua has been neglected. The energy of the continuum electron has been put equal to the calculated energy difference between the centers of gravity of the initial state and the final (ionic) state, and it has been checked that the dependence on the energy of the continuum electron is fairly small. As explained already, the Slater integrals have been scaled down to 80% in the calculations in order to reproduce the observed energies, while spin-orbit integrals and the interaction integrals with the continua have been used without any scaling.

Table I shows that there is a difference of a factor of about 100 between the decay rates for the low- and high-spin states in the SCA approximation. If only SCK is considered the factor is much larger, about 5×10^4, as expected on the basis of the good LS coupling for the septet. The decay involving two 4s electrons has a rate equal to 7.4×10^{10} s^{-1} for all states, i.e. much slower than the CK and SCK decays, and has not been included in the table. Finally, for the highest ^5P term, (^6S) ^5P, a rather unusual decay is possible since this term is located above the lowest limit for simultaneously ionizing a $3p$ and an outer $4s$ electron. This means that the decay $3p^5(3d^5\,{}^6S)4s^2\,{}^5P \rightarrow 3p^5(3d^5\,{}^6S)\,(^7P)\,4s\,{}^6P + ks$ is possible and, since it involves a fairly small free electron energy k, this decay could be expected to be important. It is included in Table I under the heading ''direct.'' Although not negligible, it turns out not to contribute very much to the total linewidth of the uppermost ^5P term. For the lower terms this decay is energetically forbidden. The SCA numbers in Table I are averages over the results for the levels belonging to a particular term. However, in the SCA the differences between individual levels are rather small.

Introduction of CI does have a considerable influence on the decay rates, increasing the linewidth of the ^7P term by a factor of 4 as shown in the table under the heading ''CI.'' This calculation includes the configurations $3p^5 3d^5 4s^2 + 3p^5 3d^6 4s + 3p^5 3d^7 + 3p^3 3d^7 4s^2 + 3s 3p^5 3d^6 4s^2$ for the initial state. The reason for the choice of configurations is that the mixing between $3d$ and $4s$ electrons is well known to be important in optical spectra, because of the small energy difference between the $3d$ and $4s$ electron in near-neutral atoms, while the $3p^2 \rightarrow 3d^2$ and $3s \rightarrow 3d$ excitations are expected to be among the most important excitations contributing to core-valence correlation. Table I shows that for the ^7P term the CK rates, in particular, are influenced by the introduction of CI. The reason is that the admixed $3p^5 3d^6 4s$ components have a very large (SCK) decay to $3p^6 3d^4 4s$ which boosts the CK decay of $3p^5 3d^5 4s^2$. Also, for the lower ^5P terms this effect leads to a significant increase in the decay rate, while for the highest ^5P term, for which the decay is already very fast, the effect is negligible.

In the CI calculations, the individual final state continua have been considered separately, while the effect of including the CI between the final ionic states in the calculations was found to be small. The free electron energy has, as in the SCA calculations, been fixed at the HFR energy difference between the centers of gravity of the initial and final (ionic) configurations. The effect of coupling the continua has been neglected but is believed to be small as far as total widths are concerned at the rather large electron energies involved. It turns out that, while the $3d^5\,{}^6S$ term is located well below all other terms in the neutral Mn spectrum, $3d^6(^5D)4s\,{}^6D$ becomes the lowest term, in the SCA, when a $3p$ electron is removed. This makes the Mn II spectrum very dense and an accidental degeneracy between, for example, a $3d^6 4s$ term and one of the $3d^5 4s^2\,{}^{5,7}P$ terms can change the excitation spectrum considerably. Since the distance between the two configurations is not accurately known, the high density of states can easily lead to artificial degeneracies and thus misleading results. The experimental spectrum indicates rather strongly that the ^7P term is intact, so that degeneracies with this term should be avoided (for example, by a suitable displacement of one or more of the configurations involved). However, for the ^5P terms it is harder to decide whether a degeneracy with $3d^6 4s$, for example, is an artifact, and the CI calculations indicate a splitting of some levels belonging to all three ^5P terms, which might be real and could lead to a reduction in the probability for excitation compared to the

SCA prediction. The rates given in Table I are again obtained by averaging, but this time the average is over all levels with a significant ^5P component. For the two lower ^5P terms, in particular, the average is over a rather large number of states, making the average value less significant.

One difference between atoms and solids is the delocalization of the $4s$ electron in the solid. In the atom, the decay rate of the high-spin states is mainly due to the normal CK decay involving a $4s$ electron. This possibility is strongly suppressed in the solid and Kotani and co-workers have usually restricted themselves to calculation of the SCK rates. The restriction on the SCK decay due to the spin-selection rule is operative for elements up to the half filled $3d$ shell. Kotani and co-workers have also found a term dependence of the decay rates in Ni [30], for example, where the shell is nearly full. The existence of this ''effective'' spin dependence, mentioned earlier, is supported by the present results, where the SCA calculations show that for the CK decay in Mn, for which the spin-selection rule has no effect, the decay rate for the $(^6S)\,^5P$ term nevertheless is 16 times larger than the decay rate for $(^6S)\,^7P$. The effect is reduced when CI is included.

We mentioned earlier that for the $3s$ spectrum McGuire [28] found a spin dependence that largely disappeared when CI was introduced. However, we have also mentioned that SCK decay is allowed for both the ^7S and the ^5S terms in the $3s$ spectrum. McGuire therefore was concerned with an effective spin dependence of the above type, a much weaker effect than the spin dependence induced by spin-selection rules. Therefore CI could largely neutralize the spin dependence. In fact we find that the difference in free electron energy between ^7S and ^5S already has an equalizing effect on the decay rates in the $3s$ spectrum.

A similar effect is important for understanding the $3p$ excitation spectrum since, in addition, a Cooper minimum exists in the $3p \rightarrow kd$ transition probability.

D. Excitation spectrum

For a proper understanding of the photoionization process, it is important also to understand the excitation spectrum, in particular the strength of the observed peaks. It was mentioned earlier that in the simplest approximation the ratio between the intensities of the septet and quintet peak(s) should be equal to the statistical degeneracy 7/5. However, we have just mentioned that the ''effective'' spin dependence of the decay rates for $3s$, for example, will make the FWHM of the ^5S peak larger, an effect that needs to be taken into account when comparing with experiment. Since there is a considerable perturbation of the ^5S term in the $3s$ spectrum, the ratio should in addition be modified with the percentage of the $3s3p^6(3d^5\,^6S)\,^5S$ component in the appropriate level, and we pointed out in the last section that there is a dependence on the energy of the photoelectron also. Although we do not know of a calculation including all these factors, the agreement of the existing estimates [25] with the the experimental data [19], which show a fairly constant ratio of about 2.4 independent of photon energy except very close to threshold, is reasonable, in particular when it is kept in mind that the $3s$ photoionization cross section as such is fairly small and therefore difficult to calculate precisely.

The $3p$ spectrum is considerably stronger but more complicated. For one thing, the cross section for photoionization of a $3p$ electron shows a rather pronounced Cooper minimum [19] and, because the energy of the outgoing electron is rather different for the ^7P and the high ^5P terms, the cross sections can be expected to have their minima at different photon energies, corresponding roughly to the same electron energy. Since the higher term, ^5P, reaches the Cooper minimum at a higher photon energy than the (lower) ^7P term, this effect contributes to increasing the ratio between the ^7P and, in particular, the high ^5P at the photon energy relevant here. Finally, the different linewidths of the septet and quintet terms must be taken into account.

We have carried out calculations of the probabilities for photoionization of the individual terms. Table II shows the relative line strengths for the individual peaks in Mn calculated in the SCA and CI approximation for different electron energies. Assuming a common electron energy, the SCA leads to a ratio between the lowest and highest terms in Mn equal to 1.9, mainly due to the transfer of $3p^5(3d^5\,^6S)\,^5P$ character to the lower $3p^5(3d^5\,^4D)\,^5P$ term. Inclusion of CI does, as surmised by McGuire [28], lead to a reduction of the ratio but, as pointed out already, the effect is much less important than for the $3s$ spectrum. In fact, if the same electron energy is used for both peaks the reduction is very small, while if this restriction is relaxed the ratio is increased instead, as mentioned above.

We have performed CI calculations including the configurations $3p^63d^54s^2+3p^63d^64s+3p^63d^7+3p^43d^74s^2+3s3p^63d^64s^2$ to describe the neutral atom and the configurations $3p^53d^54s^2+3p^53d^64s+3p^53d^7+3p^33d^74s^2+3s3p^53d^64s^2$ to describe the ion, adding a continuum d electron, which is more important than excitation via an s wave, for the calculation of the photoionization rates. Only the f values corresponding to the ^7P and the uppermost ^5P terms are shown. As mentioned earlier, the ^5P terms are spread over a number of levels in the CI calculation, and this applies particularly to the lower terms. The results in Table II correspond to the use of a fixed electron energy chosen as the difference between the mean energies of the two configurations involved, as well as to the use of different electron energies to determine the cross sections for the two terms separately. The relative intensities within the ^7P multiplet are unchanged by the introduction of CI and the same applies to the energy separations in the multiplet. However, the intensity of the uppermost ^5P multiplet is spread over a number of levels and for this reason only the sum of individual f values is shown. The two different electron energies in the columns of relative f values correspond to the actual ^7P electron energy, 65 eV, at a photon energy of 122 eV and the actual ^5P energy, 47 eV, at the same photon energy. The value for ^5P at 47 eV is calculated relative to the f value for ^7P at 65 eV. Thus the ratio (2.6) between ^5P at 47 eV and ^7P at 65 eV is the most accurate intensity ratio reported here.

Energies and relative line strengths have also been calculated for Cr within the SCA and the CI approximation. The

TABLE II. Assignments, binding energies (experimental uncertainties in parentheses), and relative line strengths of the lines observed in the $3p$ photoelectron spectrum of Mn atoms. The calculations use scaling of the interaction integrals (see text). The relative f values in the CI approximation are obtained at two different free electron energies ϵ corresponding to the decays of $(^6S)\,^7P$ and $(^6S)\,^5P$, respectively, see text.

		Experiment	SCA		CI		
Label[a]	Mn II state	Energy (eV)	Energy (eV)	Rel. f value	Energy[b] (eV)	Rel. f value $\epsilon=65$ eV	$\epsilon=47$ eV
A	$3p^5(3d^5\,^6S)4s^2\,^7P_4$	57.04(5)	57.04[c]	1.00	57.04[c]	1.00	
	$^7P_3$	57.53(5)	57.51	0.78	57.49	0.77	
	$^7P_2$	57.97(5)	57.92	0.56	57.89	0.55	
B	$3p^5(3d^5\,^4D)4s^2\,^5P_1$		60.19	0.11	59.72		
	$^5P_2$	60.3–60.6	60.39	0.18	59.89		
	$^5P_3$		60.65	0.26	60.13		
C	$3p^5(3d^5\,^4P)4s^2\,^5P_3$		64.30	0.006	63.82		
	$^5P_2$	63.5–64.5	64.69	0.008	64.34		
	$^5P_1$		64.76	0.007	64.22		
D	$3p^5(3d^5\,^6S)4s5s\,^7P_4$	66.9(1)	66.94(5)[d]				
	$^7P_3$	67.3(1)	67.19(5)[d]				
	$^7P_2$	67.7(1)	67.71(5)[d]				
E	$3p^5(3d^5\,^6S)4s4d$	68.2(1)	68.1(1)[d]				
		68.7(1)	68.5[d]				
		69.1(1)					
F	$3p^5(3d^5\,^6S)4s^2\,^5P_1$		75.75	0.24	74.20		
	$^5P_2$	74.3–75.8	75.94	0.43	74.48	1.27	0.89
	$^5P_3$		76.27	0.56	74.83		

[a]See Fig. 1.

[b]The energy level with the largest component of the indicated eigenvector is shown, but several of the low ^5P levels in particular are very mixed; see text. The order of the levels in the $(^4P)\,^5P$ term is inverted in the CI relative to the SCA calculation for this reason.

[c]The experimental binding energy is used to calibrate the theoretical energies.

[d]Values based on energies of the Mn^+ absorption lines [35], see text.

results are summarized in Table III. CI calculations for Cr turned out to be more difficult because of the open $4s$ shell and the importance of $4s\rightarrow 4d$ excitations as explained later.

IV. RESULTS AND DISCUSSION

Since most calculations have been carried out for Mn we start by considering this atom.

A. Mn

The experimental $3p$ photoelectron spectrum of atomic Mn at a photon energy equal to 122 eV is given in the top part of Fig. 1 where the individual lines are indicated with capital letters. The sharp and prominent $3p^5(3d^5\,^6S)4s^2\,^7P$ lines at low binding energies (A) lie 18 eV below the $3p^5(3d^5\,^6S)4s^2\,^5P$ lines with the highest binding energy (F). The $3p$-$3d$ exchange interaction causes this separation of the ^7P and ^5P states where the total $3p$ spin is parallel and antiparallel to the total $3d$ spin, respectively. Recoupling of the $3d$ electrons gives rise to the ^5P lines B and C, which, as mentioned, get their strength from the electrostatic coupling with the $(^6S)\,^5P$ term. The $Z+1$ model (see top part of Fig. 1) predicts shake-up lines in the binding energy range of the lines D and E. More accurate values for the binding energies of the $5s$ and $4d$ shake-up lines have been obtained by adding the Mn ionization energy of 7.4341 eV [27] to the energies of Mn II absorption lines [35]. The $3p^53d^54s\ ^8P$ double-ionization limits shown in the figure are based on estimates of the $Mn^+\,3p$ ionization thresholds [35]. The assignments, the experimental and theoretical binding energies, and the relative line strengths are summarized in Table II, which shows the results with the lowest $(^6S)\,^7P$ level used as reference level. With the scaling factors mentioned above, the $(^6S)\,^5P$ term is calculated slightly higher than observed in the SCA calculation, while the introduction of CI moves the term below the observed position, as expected. However, the shift is not large enough to justify the use of a different set of scaling factors. Also, the lower ^5P terms are slightly too low in the CI calculation but within the accuracy of the approach the agreement is good enough to confirm the assignments of the experimental peaks. We note that scaling down the CI integrals would improve the agreement with experiment. We note that also for the $3s$ spectrum the use of unscaled CI integrals places the ^5S term too close to ^7S.

The calculated $3p^5(3d^5\,^6S)4s^2\,^7P,\ ^5P$ photoelectron lines are given by the bar diagram in the bottom part of Fig.

TABLE III. Assignments, binding energies, and relative line strengths of the features observed in the $3p$ photoelectron spectrum of atomic Cr (experimental uncertainties in parentheses). Note that the CI calculations for energies and line strengths are different, see text.

		Energies (eV)		Theory			
		Experiment	Abs. [b]	Energies (eV)		Rel. line strength	
Label[a]	Cr II state			SCA	CI	SCA	CI
A	$3p^5(3d^5\,{}^6S)({}^7P)4s\,{}^8P_{9/2}$	46.34(5)		46.34 [c]	46.34 [c]	1.0	1.0
	${}^8P_{7/2}$	46.70(5)		46.70	46.69	0.80	0.80
	${}^8P_{5/2}$	47.03(5)		47.02	47.01	0.60	0.60
B	$3p^5(3d^5\,{}^6S)({}^7P)4s\,{}^6P_{7/2}$		47.67(5)	47.73	47.71	0.02	0.02
	${}^6P_{5/2}$		48.05(5)	48.10	48.07	0.02	0.02
	${}^6P_{3/2}$		48.35(5)	48.40	48.35	0.02	0.02
C	$3p^5(3d^5\,{}^4D)({}^5P)4s\,{}^6P_{3/2}$			49.26	48.83	0.12	0.12
	${}^6P_{5/2}$	49.6	49.52(5)	49.39	48.95	0.19	0.19
	${}^6P_{7/2}$		49.65(5)	49.58	49.13	0.26	0.26
D	$3p^5(3d^5\,{}^6S)({}^7P)4p$	50.4–52		51.3			
E	$3p^5(3d^5\,{}^4P)({}^5P)4s\,{}^6P_{7/2}$			52.93	52.33	0.007	0.007
	${}^6P_{5/2}$	53–54		53.18	52.44	0.007	0.005
	${}^6P_{3/2}$			53.23	52.65	0.006	0.005
F	$3p^5(3d^5\,{}^6S)({}^7P)5s\,{}^6P_{7/2}$		55.55(5)				
	${}^8P_{7/2}$		55.71(5)				
	${}^6P_{5/2}$	55.4	55.91(5)	55.5			
	${}^8P_{5/2}$		56.04(5)				
	${}^6P_{3/2}$		56.26(5)				
	$3p^5(3d^5\,{}^6S)({}^7P)4d\,{}^8P_{5/2}$				55.46		
	${}^8P_{7/2}$	55.8			55.50		
	${}^8P_{9/2}$				55.80		
G	$3p^5(3d^5\,{}^6S)({}^5P)4s\,{}^6P_{3/2}$	60.8(2)		63.14	61.83	0.29	0.29
	${}^6P_{5/2}$			63.30	61.95	0.45	0.45
	${}^6P_{7/2}$	61.8(2)		63.54	62.18	0.56	0.56
H		64–64.8					
I		65.2–66.2					

[a]See Fig. 3.

[b]The binding energies are based on the energies of the Cr^+ absorption lines [40]; see text.

[c]The theoretical binding energy has been matched to the experimental value.

1. The lengths of the bars are proportional to the f values obtained in the SCA. The energy positions correspond to CI binding energies. There is at first sight an obvious discrepancy between experiment and theory concerning the relative amplitudes of the lines. However, these amplitudes are strongly influenced by the term-dependent linewidth as discussed already. The SCK decay, forbidden for the low-energy ${}^7P$ lines, gives rise to a dramatic broadening of the high-energy ${}^5P$ lines. The calculated widths of the lines caused by CK and SCK decays are presented in Table I. In order to facilitate the comparison with the experimental spectrum, we convoluted the bar spectrum (bottom part of Fig. 1) with a Lorentzian and a Gaussian profile. By choosing the width of the Lorentzians equal to the calculated CI linewidths (Table I) and the width of the Gaussian equal to the instrumental resolution, the spectrum in the center part of Fig. 1 was generated. This spectrum describes the main features of the experimental spectrum reasonably well, especially the dramatic reduction of the amplitude of the high-energy ${}^5P$ lines. We note that the use of the f values obtained in the CI approach, including the effect of the difference in free electron energy between the ${}^7P$ and the high ${}^5P$ terms (last two columns of Table II), would reduce the height of the ${}^5P$ peak in the center part of Fig. 1 further and improve the agreement with experiment as discussed below. From the photoelectron lines and the $3p^53d^54s^2\,{}^7P$–$3p^63d^44s\,{}^6D$ Auger lines an experimental width of 140 meV ± 20 meV has been extracted, in good agreement with the CI value of 130 meV in Table I but much larger than the SCK rate even when CI is included.

We have already pointed out that the intensity ratio between the features A and F is strongly photon energy dependent. The ratio, which can be determined from Fig. 1, is approximately equal to 7 in good agreement with the results of Jiménez-Mier *et al.* [19]. The SCA calculations used in Fig. 1 predict a value of 1.9 for the ratio of the total line strength of the low-energy ${}^7P$ line and the total line strength

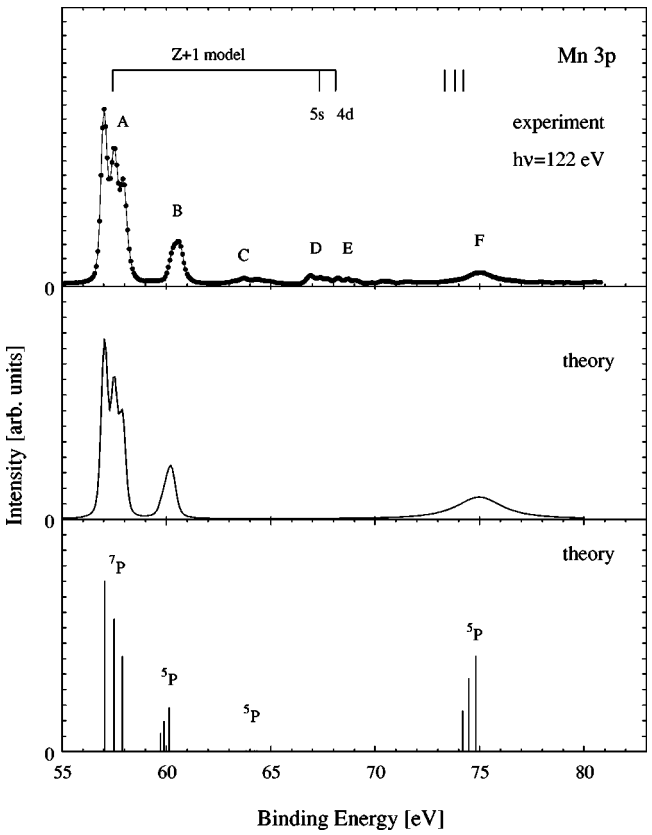

FIG. 1. Top part: Experimental $3p$ photoelectron spectrum of atomic Mn taken at a photon energy of 122 eV. The peaks labeled by capital letters are discussed in the text. The energy positions of the Mn II $3p^5 3d^5 4snl$ shake-up states predicted by the $Z+1$ model are indicated. Center and bottom parts: Calculated Mn II $3p^5 3d^5 4s^2\,{}^7P$, ^5P photoelectron lines. The strength of the lines was calculated within the single-configuration approximation and is given by the lengths of the bars in the lower part. Convoluting this bar spectrum with Lorentzian and Gaussian profiles, the spectrum in the center part was obtained. The widths of the Lorentzians were chosen equal to the calculated linewidths in the CI approximation (Table I) while the width of the Gaussian was determined by the instrumental resolution. The energies were calculated within the CI approximation. The energy of the strongest $3p^5(3d^5\,{}^6S)4s^2\,{}^7P_4$ line has been matched to the energy of the strongest line of group A.

of the high-energy ^5P line. However, if the difference in electron energy between the two peaks is taken into account, a ratio somewhat larger than 2 is obtained (Table II). It turns out that in the single-configuration HFR approximation the Cooper minimum is located at a lower energy than experimentally observed. If we correct for this by using a smaller electron energy to determine the cross sections, then the theoretical value comes close to the large value observed experimentally. In fact, the main remaining problem is the high-energy limit of this ratio. Experimentally at 240 eV it has been determined to be close to 4 [19] while our value with the same electron energy for each peak is close to 2, essentially independent of photon energy in the limited energy range studied. It is interesting that in the calculations published by Amusia *et al.* [36] of the branching ratio for $4s$

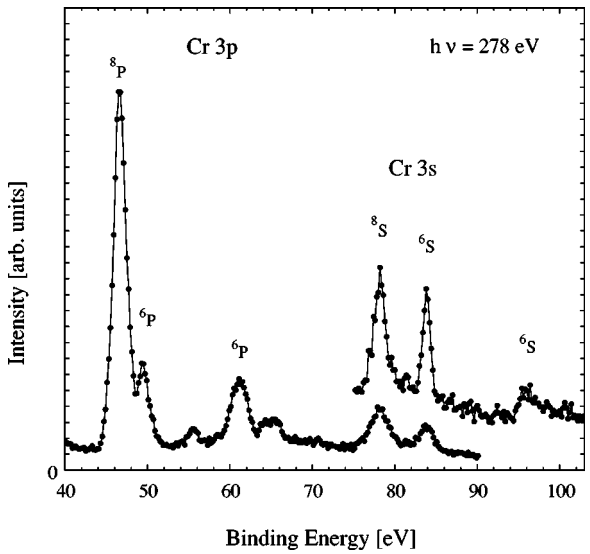

FIG. 2. Experimental $3p$ and $3s$ photoelectron spectra of atomic Cr taken at a photon energy of 278 eV. The assignment of the strongest photoelectron lines to Cr II $3p^5 3d^5 4s\,{}^8P$ and ^6P and Cr II $3s3p^6 3d^5 4s\,{}^8S$ and ^6S final states is indicated.

ionization a similar effect is visible. Amusia *et al.* have shown that the effect of the $3p \rightarrow 3d$ excitation on the $4s$ ionization is strong and can explain the deviation in the ratio between the ^7S and ^5S peaks for the $4s$ ionization [37]. However, the calculation show a fast decrease in the branching ratio from about 70 eV photon energy, whereas the experimental ratio [37,38] reaches its maximum at 80 eV and stays considerably above the calculated value up to 90 eV, i.e., the limit of the calculation.

B. Cr

There has been a considerable interest in comparing the photoabsorption spectra of Cr and Mn [39]. It has been found that the two spectra are rather different, with the Cr spectrum showing considerably more detail than is the case for Mn. Costello *et al.* [40] have compared not only the absorption spectra of the neutral atoms but also those of the singly ionized species. They concluded that in Cr there is a mixing of Rydberg states belonging to $3p^5 3d^5 4d$ with $3p^5 3d^6$, which is not present in Mn. We have found that there is more structure in the photoionization cross section of Cr than for Mn and we surmise that a possible reason is the admixture of $3p^5 3d^5 4d$ states. Although this interpretation looks reasonable when combined with the earlier evidence for the importance of this configuration, we note that the features we are trying to identify are very weak and that the spectrum is very complicated with many overlapping configurations.

Figure 2 shows an overview spectrum taken with a moderate photoelectron resolution ($\Delta E = 1.7$ eV; inset has $\Delta E = 0.7$ eV) at a photon energy of 278 eV. The Cr $3p$ photoelectron lines span the binding energy range from 42 eV to 66 eV while the strongest Cr $3s$ photoelectron lines show up at 78.2 ± 0.1 eV $[3s3p^6(3d^5\,{}^6S)\,({}^7S)4s\,{}^8S]$ and 83.8 ± 0.1 eV $[3s3p^6(3d^5\,{}^6S)\,({}^5S)4s\,{}^6S]$. The $3s$ spectrum closely resembles the 3s photoelectron spectrum of atomic

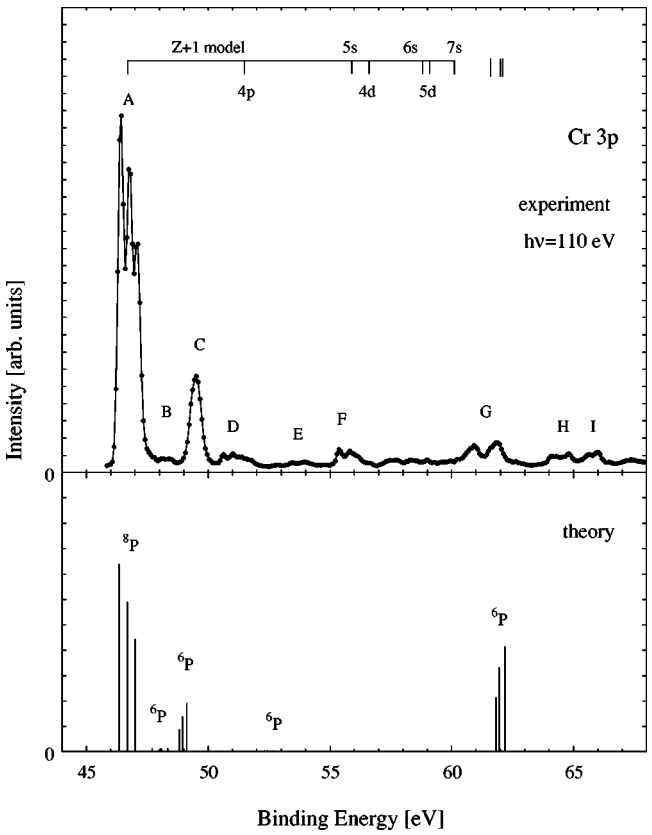

FIG. 3. Upper part: Experimental $3p$ photoelectron spectrum of atomic Cr taken at a photon energy of 110 eV. The energy positions of the Cr II $3p^5 3d^5 nl$ shake-up states predicted by the $Z+1$ model and the $3p^5 3d^5\,{}^7P$ double ionization limits are indicated. Lower part: Calculated Cr II $3p^5 3d^5 4s\,{}^8P$ and ${}^6P$ photoelectron lines. The energies are calculated within the CI approximation. The strength of the lines calculated within the SCA is given by the lengths of the bars. The energy of the strongest $3p^5(3d^5\,{}^6S)4s\,{}^8P_{9/2}$ line has been matched to the energy of the strongest line of group A.

Mn [17,19] and therefore we ascribe the line at 96.2 ± 0.2 eV to a $3s^2 3p^4 3d^6 4s$ satellite gaining its strength from the admixture of $3s3p^6(3d^5\,{}^6S)({}^5S)4s\,{}^6S$. The $3s3p^6(3d^5\,{}^6S)({}^7S)4s\,{}^8S$ line is asymmetric because of the nearby $3s3p^6(3d^5\,{}^6S)({}^7S)4s\,{}^6S$ line, which is absent in the spectrum of atomic Mn. It is calculated about 1.5 eV above the ${}^8S$ line but, judging from the inset in Fig. 2, the real distance is perhaps a little smaller.

Here we concentrate on the $3p$ photoelectron spectrum, which comprises several components as demonstrated by the photoelectron spectrum taken with higher resolution (A–I, Fig. 3). This spectrum is shown in the upper part of Fig. 3 where the three spin-orbit-split components $3p^5(3d^5\,{}^6S)({}^7P)4s\,{}^8P_{9/2,7/2,5/2}$ of line A are clearly resolved. Fine structure can also be observed for the lines D, F, G, H, and I. The $3p$-$3d$ exchange interaction spreads the $3p^5 3d^5 4s\,{}^8P$, ${}^6P$ multiplet lines over more than 15 eV. The results of the CI calculations for the binding energies and those of the SCA calculations for the relative line strength are given by the bar diagram in the lower part of Fig. 3. The interpretation is similar to that for Mn except that the unpaired spin of the $4s$ electron gives rise to the weak group B, where the $4s$ spin has been flipped relative to the A group. The groups C and E represent the recoupling of the $3d^5$ shell. The additional lines D and F are assigned to $3p^5 3d^5 nl$ shake-up states. An estimate for the energy of the shake-up lines is provided by the $Z+1$ model indicated in the upper part of Fig. 3. These predictions are corroborated by SCA calculations and by experimental binding energies obtained by adding the 6.7667 eV ionization potential [27] of Cr to the energies of Cr^+ absorption lines [40]. Experimental binding energies for the groups B and C have been obtained in the same way. We notice that the SCA energies for the $3p^5(3d^5\,{}^6S)({}^5P)4s\,{}^6P$ levels using the same scaling as for Mn are below the energies associated with the features H and I. The predicted energies are, however, somewhat larger than those corresponding to the features G, but we nevertheless have assigned G to the $3p^5(3d^5\,{}^6S)({}^5P)4s\,{}^6P$ term. The main reason is the following. Comparing the spectra in Figs. 2 and 3, we see that the feature G is much stronger relative to C in Fig. 2 (photon energy 278 eV) than in Fig. 3 (photon energy 110 eV). This behavior corresponds to the behavior of the ${}^7P/{}^5P$ intensity ratio in Mn. For the H and I peaks the intensity seems less dependent on the photon energy. As a further confirmation we have carried out CI calculations of the energy spectrum including the $3p^5 3d^5 4s + 3p^5 3d^5 4d + 3p^5 3d^6 + 3p^5 3d^4 4s^2$ configurations and adding the $3s \rightarrow 3d$ and $3p^2 \rightarrow 3d^2$ excitations for the first three configurations. These fairly large-scale calculations (matrix sizes up to 2085×2085 for $J=5/2$) show that the $3p^5(3d^5\,{}^6S)({}^5P)4s\,{}^6P$ term is pushed considerably farther down than the low ${}^8P$ term and, using the same scaling as for Mn, there is now reasonable agreement with the observed energies (Table III). The calculated $3p^5(3d^5\,{}^6S)({}^5P)4s\,{}^6P$ energy is still slightly too high, while the low $({}^4P)$ and $({}^4D)\,{}^6P$ terms are too low. The latter was also observed in Mn. We note that the structure G is very close to the $3p^5 3d^5\,{}^7P_4$ (61.6 eV), $3p^5 3d^5\,{}^7P_3$ (62.0 eV), and $3p^5 3d^5\,{}^7P_2$ (62.3 eV) double-ionization limits [40]. It is not clear why G is double, although the possibility exists that the $3p^5(3d^5\,{}^6S)({}^5P)4s\,{}^6P$ term is spread over a number of levels as mentioned earlier. There are many predicted energy levels in the region of the H and I peaks but an assignment is difficult. Calculations of the excitation spectrum are also difficult, not only because the open $4s$ shell leads to larger matrices but also because it is necessary to add the $3d^5 4d$ configuration. This leads to very large matrices, and we have carried out calculations using $3p^6 3d^5 4s + 3p^6 3d^5 4d + 3p^6 3d^4 4s^2 + 3p^6 3d^6$ for the initial state and $3p^5 3d^5 4s + 3p^5 3d^5 4d + 3p^5 3d^4 4s^2 + 3p^5 3d^6$ coupled to a continuum d electron for the final state. The free electron energy is 57.3 eV, corresponding to a photon energy of 110 eV for the center of gravity of the $3p^5 3d^5 4s$ configuration. The resulting matrices are so large, up to 4269×4269, that no attempt was made to include the excitations from the $3p$ and $3s$ shells in this case. The results in Table III do not show appreciable strength for any $4d$ level, but this is perhaps due to the omission of the inner shell excitations. These excitations do lead to appreciable mixing in the wave functions. For example, in the CI calculation of the energy spectrum the

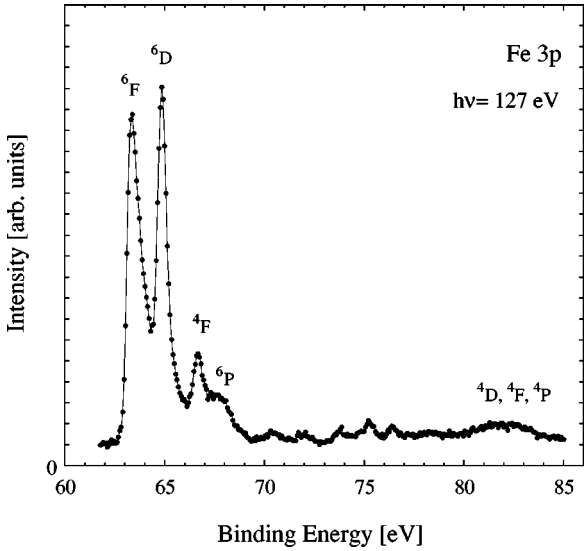

FIG. 4. Experimental $3p$ photoelectron spectrum of atomic Fe taken at a photon energy of 127 eV. The assignment of the strongest lines to the Fe II $3p^5 3d^6 4s^2\,{}^6L$ and ${}^4L$ final states is indicated.

$3p^5(3d^5\,{}^6S)({}^5P)4s\,{}^6P$ term is only 60% pure in the $3p^5 3d^5 4s$ label. Taking this fully into account can be expected to change the excitation spectrum in the last column of Table III, but it would require very large calculations.

The assignments of the Cr photoelectron lines, the experimental and theoretical binding energies, and the theoretical line strengths are summarized in Table III. With respect to binding energies there is, as mentioned, reasonable agreement between the experimental and theoretical values with the feature G assigned to $3p^5(3d^5\,{}^6S)({}^5P)4s\,{}^6P$. The width of the $3p$ photoelectron lines is strongly term dependent. The Cr^+ $3p^5(3d^5\,{}^6S)({}^7P)4s\,{}^8P$ term cannot undergo neither CK nor SCK decay if pure. High-resolution Auger spectra [41] indicate a linewidth of about 10 meV, considerably narrower

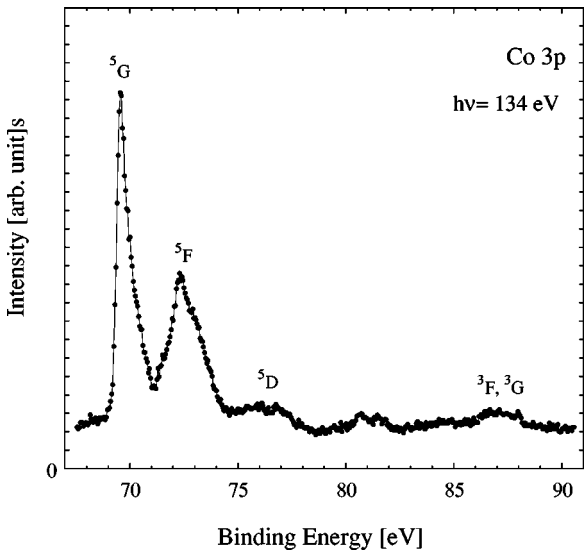

FIG. 5. Experimental $3p$ photoelectron spectrum of atomic Co taken at a photon energy of 134 eV. The assignment of the strongest lines to the Co II $3p^5 3d^7 4s^2\,{}^5L$ and ${}^3L$ final states is indicated.

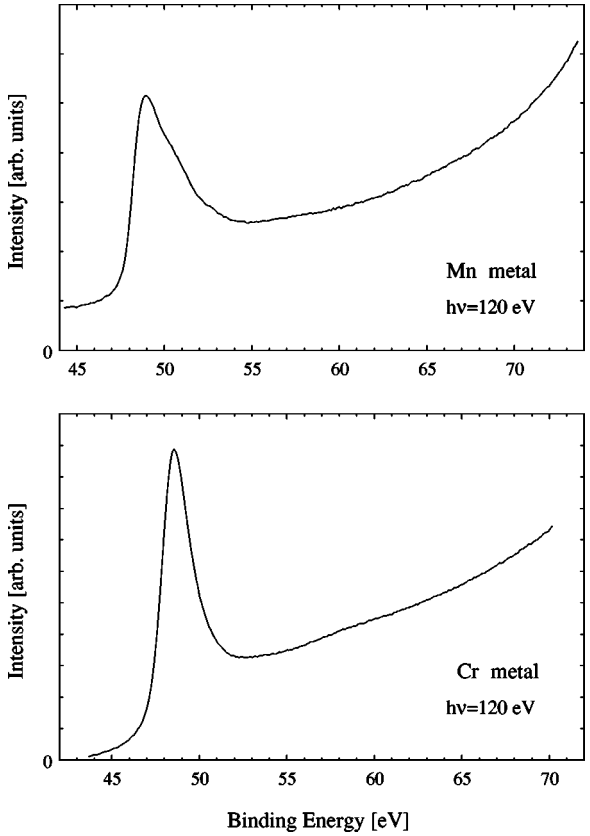

FIG. 6. Experimental $3p$ photoelectron spectra of Mn metal (upper part) and Cr metal (lower part) taken at a photon energy of 120 eV.

than the ${}^7P$ lines in Mn. This observation thus supports our earlier conclusion concerning Mn, where primarily the CI induced CK decay is responsible for the observed linewidth. The width of the ${}^8P$ lines in Fig. 3 is determined by the instrumental resolution. The width of approximately 0.5 eV of each component of the structure G is also less than expected for the $3p^5(3d^5\,{}^6S)({}^5P)4s\,{}^6P$ term on the basis of the Mn results.

C. Fe and Co

The $3p$ photoelectron spectra of Fe and Co atoms are displayed in Figs. 4 and 5. The Fe $3p^5 3d^6 4s^2\,{}^{6,4}L$ and the Co $3p^5 3d^7 4s^2\,{}^{5,3}L$ multiplet lines span an energy range of almost 20 eV. The assignment of the corresponding photoelectron lines is indicated in the figures. The $3p$-$3d$ exchange interaction places the states with the total $3p$ spin parallel to the total $3d$ spin at low binding energies and those with the opposite relative orientations of the total $3p$ and $3d$ spins at high binding energies. The term dependence of the lifetime broadening by CK and SCK decays clearly manifests itself in the prominent lines at low and the weak and broad structures at high binding energies, even though the simple explanation in terms of the SCK transitions being forbidden for the high-spin states is no longer valid, as mentioned earlier. For Fe, the assignment of the lines at low binding energies is supported by photoelectron spectra taken

with better resolution [22]. For a detailed discussion of the Fe and Co $3p$ photoelectron spectra, see [42].

D. Cr and Mn metal

In Fig. 6 the $3p$ photoelectron spectra of Mn (upper part) and Cr metal (lower part) are shown. The binding energy is referred to the vacuum level. In order to reduce the statistical fluctuations up to 10^5 counts have been accumulated per channel. Both spectra display a prominent, asymmetric photoelectron line several eV wide at low binding energies. For Mn the small shoulder on the high-energy side is due to oxygen contamination of the surface layer. Toward higher binding energies, the intensity increases smoothly due to the background of scattered electrons not corrected for. Above the peak the Mn spectrum does not show any significant structure. There is an indication of a very weak maximum centered at 58 eV in the spectrum of Cr.

Transferring the results obtained for the free atoms to the metals offers an obvious explanation for the lack of any significant structures at binding energies above the prominent low-energy peak. Due to the considerable lifetime broadening the corresponding structures are already very weak in the spectra of the free atoms. Additional solid state broadening can result in an almost complete suppression of the high-energy structures. Remember that the highest ^5P term in Mn is located above the lowest limit associated with removing a $3p$ electron from the core, basically the Fermi level in the metal. The barely visible structure in the spectrum of Cr metal could be due to a surface plasmon. Before drawing further conclusions from the comparison of atomic and metallic spectra it is essential to list a number of caveats. The partial delocalization of the d electrons, the formation of the $4s$ conduction bands, different and even intermediate fractional occupation numbers, screening, and relaxation are the most important solid state effects. Despite these complications it is hard to accept that the $3p$-$3d$ exchange interaction can be reduced by more than one order of magnitude in the metals. Such a reduction is implied by assigning the prominent line in the metal photoelectron spectra to $3p_{1/2,3/2}$ hole states, as has been done in several recent publications concerning dichroism effects in metals [11–14]. Comparison of the atomic and metallic spectra suggests instead that the peaks observed in the metals should be described by those multiplet states of the $3p$ ionized transition metal ions in which the total $3p$ spin is parallel to the total $3d$ spin. The validity of this multiplet-hole approach has been demonstrated for $3d$ metals (e.g., [2,15,20]) and for $3d$ metal compounds [10,17,43]. The $3p$ absorption spectra of the free atoms and the corresponding metals provide further clear evidence for the strong influence of the $3p$-$3d$ interaction on the $3p$ spectra of the $3d$ transition metals ([19,23,44,45] and references therein).

ACKNOWLEDGMENTS

The work of J.E.H. was sponsored by the Stichting Nationale Computerfaciliteiten (National Computing Facilities Foundation, NCF) for the use of supercomputer facilities, with financial support from the Nederlandse Organisatie voor Wetenschappelijk Onderzoek (Netherlands Organization for Scientific Research, NWO). The financial support of the Deutsche Forschungsgemeinschaft and the continuous assistance of the BESSY and HASYLAB staff are gratefully acknowledged.

[1] C. Carbone and E. Kisker, Solid State Commun. **65**, 1107 (1988).
[2] T. Kachel, C. Carbone, and W. Gudat, Phys. Rev. B **47**, 15 391 (1993).
[3] F.U. Hillebrecht, Ch. Roth, R. Jungblut, E. Kisker, and A. Bringer, Europhys. Lett. **19**, 711 (1992).
[4] Ch. Roth, F.U. Hillebrecht, H.B. Rose, and E. Kisker, Phys. Rev. Lett. **70**, 3479 (1993).
[5] F. Sirotti and G. Rossi, Phys. Rev. B **49**, 15 682 (1994).
[6] E. Tamura, G.D. Waddill, J.G. Tobin, and P.A. Sterne, Phys. Rev. Lett. **73**, 1533 (1994).
[7] Di-Jing Huang, D.M. Riffe, and J.L. Erskine, Phys. Rev. B **52**, 15 170 (1995).
[8] Ch. Roth, Th. Kleeman, F.U. Hillebrecht, and E. Kisker, Phys. Rev. B **52**, R15 691 (1995).
[9] Zhongde Xu, Y. Liu, P.D. Johnson, and B.S. Itchkawitz, Phys. Rev. B **52**, 15 393 (1995).
[10] M. Taguchi, T. Uozumi, and A. Kotani, J. Phys. Soc. Jpn. **66**, 247 (1997).
[11] G. Rossi, G. Panaccione, F. Sirotti, and N.A. Cherepkov, Phys. Rev. B **55**, 11 483 (1997).
[12] M. Liberati, P. Prieto, and G. Rossi, Phys. Rev. B **59**, 4201 (1999).
[13] N.A. Cherepkov, Phys. Rev. B **50**, 13 813 (1994).
[14] G. van der Laan, Phys. Rev. B **51**, 240 (1995).
[15] P.S. Bagus and J.V. Mallow, Chem. Phys. Lett. **228**, 695 (1994).
[16] B. Sonntag and P. Zimmermann, Rep. Prog. Phys. **55**, 911 (1992).
[17] B. Hermsmeier, C.S. Fadley, M.O. Krause, J. Jiménez-Mier, P. Gerard, and S.T. Manson, Phys. Rev. Lett. **61**, 2592 (1988).
[18] R. Malutzki, M.S. Banna, W. Braun, and V. Schmidt, J. Phys. B **18**, 1735 (1985).
[19] J. Jiménez-Mier, M.O. Krause, P. Gerard, B. Hermsmeier, and C.S. Fadley, Phys. Rev. A **40**, 3712 (1989).
[20] A. von dem Borne, T. Dohrmann, A. Verweyen, B. Sonntag, K. Godehusen, and P. Zimmermann, Phys. Rev. Lett. **78**, 4019 (1997).
[21] K.J. Ross and B. Sonntag, Rev. Sci. Instrum. **66**, 4409 (1995).
[22] Ch. Gerth, K. Tiedtke, M. Martins, B. Obst, P. Zimmermann, P. Glatzel, A. Verweyen, Ph. Wernet, and B. Sonntag, J. Phys. B **31**, 2539 (1998).
[23] K. Tiedtke, Ch. Gerth, B. Kanngießer, B. Obst, P. Zimmermann, M. Martins, and A. Tutay, Phys. Rev. A **60**, 3008 (1999).
[24] C.S. Fadley, D.A. Shirley, A.J. Freeman, P.S. Bagus, and J.V.

Mallow, Phys. Rev. Lett. **23**, 1397 (1969).
[25] P.S. Bagus, A.J. Freeman, and F. Sasaki, Phys. Rev. Lett. **30**, 850 (1973).
[26] A.J. Freeman, P.S. Bagus, and J.V. Mallow, Int. J. Magn. **4**, 35 (1973).
[27] J. Sugar and C. Corliss, J. Phys. Chem. Ref. Data **14**, Suppl. 2 (1985).
[28] E. McGuire, Phys. Rev. A **10**, 32 (1974).
[29] H. Ogasawara, A. Kotani, and B.T. Thole, Phys. Rev. B **50**, 12 332 (1994).
[30] K. Okada, A. Kotani, H. Ogasawara, Y. Seino, and B.T. Thole, Phys. Rev. B **47**, 6203 (1993).
[31] V. Schmidt, Comments At. Mol. Phys. **17**, 1 (1985).
[32] R.D. Cowan, *The Theory of Atomic Structure and Spectra* (University of California Press, Berkeley, CA, 1981).
[33] R.D. Cowan and D.C. Griffin, J. Opt. Soc. Am. **66**, 1010 (1976).
[34] K. Rajnak and B.G. Wybourne, Phys. Rev. **132**, 280 (1963); Phys. Rev. **134**, A596 (1964).
[35] J.W. Cooper, C.W. Clark, C.L. Cromer, T.B. Lucatorto, B.F. Sonntag, E.T. Kennedy, and J.T. Costello, Phys. Rev. A **39**, 6074 (1989).
[36] M.Ya. Amusia, V.K. Dolmatov, and M.M. Mansurov, J. Phys. B **23**, L491 (1990).
[37] M. Meyer and B.F. Sonntag, quoted in Ref. [36].
[38] M. Talkenberg, Diplomarbeit, Universität Hamburg, 1999 (unpublished).
[39] V.K. Dolmatov, J. Phys. B **26**, L79 (1993); **26**, L585 (1993); Th. Dohrmann, A. von dem Borne, A. Verweyen, B. Sonntag, W. Wedowski, K. Godehusen, P. Zimmermann, and V. Dolmatov, *ibid.* **29**, 4641 (1996), and references therein.
[40] J.T. Costello, E.T. Kennedy, B.F. Sonntag, and C.W. Clark, Phys. Rev. A **43**, 1441 (1991).
[41] W. Benten, Diplomarbeit, TU-Berlin, 1998 (unpublished).
[42] K. Tiedtke, Ch. Gerth, B. Obst, P. Zimmermann, and M. Martins (unpublished).
[43] P.S. Bagus, R. Broer, W.A. de Jong, W.C. Nieuwpoort, F. Parmigiani, and L. Sangaletti, Phys. Rev. Lett. **84**, 2259 (2000).
[44] R. Bruhn, B. Sonntag, and H.W. Wolff, J. Phys. B **12**, 203 (1979).
[45] L.C. Davis, J. Appl. Phys. **59**, R25 (1986).